Atmos. Chem. Phys. Discuss., 15, 29639–29671, 2015
www.atmos-chem-phys-discuss.net/15/29639/2015/
doi:10.5194/acpd-15-29639-2015

Atmospheric Chemistry and Physics Discussions

The immersion freezing behavior of mineral dust particles mixed with biological substances

S. Augustin-Bauditz[1,*], H. Wex[1], C. Denjean[1], S. Hartmann[1], J. Schneider[2], S. Schmidt[2], M. Ebert[3], and F. Stratmann[1]

[1]Leibniz Institute for Tropospheric Research, Permoserstr. 15, 04318 Leipzig, Germany
[2]Max Planck Institute for Chemistry, Hahn-Meitner-Weg 1, 55128 Mainz, Germany
[3]Institute of Applied Geosciences, Schnittspahnstraße 9, 64287 Darmstadt, Germany
[*] *Invited contribution by S. Augustin-Bauditz, recipient of the EGU Outstanding Student Poster (OSP) Award 2014.*

Received: 2 September 2015 – Accepted: 25 September 2015 – Published: 30 October 2015

Correspondence to: S. Augustin-Bauditz (augustin@tropos.de)

Published by Copernicus Publications on behalf of the European Geosciences Union.

Abstract

Biological particles such as bacteria, fungal spores or pollen are known to be efficient ice nucleating particles. Their ability to nucleate ice is due to ice nucleation active macromolecules (INM). It has been suggested that these INM maintain their nucleating ability even when they are separated from their original carriers. This opens the possibility of an accumulation of such INM in e.g., soils, resulting in an internal mixture of mineral dust and INM. If particles from such soils which contain biological INM are then dispersed into the atmosphere due to wind erosion or agricultural processes, they could induce ice nucleation at temperatures typical for biological substances, i.e., above −20 up to almost 0 °C. To explore this hypothesis, we performed a measurement campaign within the research unit INUIT, where we investigated the ice nucleation behavior of mineral dust particles internally mixed with INM. Specifically, we mixed a pure mineral dust sample (illite-NX) with ice active biological material (birch pollen washing water) and quantified the immersion freezing behavior of the resulting particles utilizing the Leipzig Aerosol Cloud Interaction Simulator (LACIS). To characterize the mixing state of the generated aerosol we used different methods which will also be discussed. We found that internally mixed particles, containing ice active biological material, follow the ice nucleation behavior observed for the purely biological particles, i.e. freezing occurs at temperatures at which mineral dusts themselves are not yet ice active. It can be concluded that INM located on a mineral dust particle determine the freezing behavior of that particle.

1 Introduction

In the last years a lot of effort has been made to characterize the freezing ability of different aerosol particles, which were thought to be ice nucleating active. Especially mineral dust particles were investigated quite intensively, as they were found in ice crystal residues most frequently (Kumai, 1961; DeMott et al., 2003; Pratt et al., 2009).

ACPD
15, 29639–29671, 2015

Laboratory measurements indicate that mineral dust particles are efficient ice nucleating particles in a temperature range below −15 °C (Murray et al., 2012) or probably only below −20 °C (Augustin-Bauditz et al., 2014), where the latter examined particles with atmospherically relevant sizes. In contrast, atmospheric observations with lidar and radar showed that ice particles also formed at higher temperatures (Seifert et al., 2010; Kanitz et al., 2011; Bühl et al., 2013). It has been assumed in the past, that the presence of biological particles like bacteria, fungal spores or pollen is necessary to explain ice nucleation at higher temperatures, as these particles show ice nucleation ability up to temperatures of −2 °C (Maki et al., 1974; Morris et al., 2008). Only comparatively recent it became known that biological particles carry small ice nucleating macromolecules (INM) which are responsible for their freezing ability. These INM could be e.g., proteins in case of bacteria (Wolber et al., 1986) and fungal spores (Fröhlich-Nowoisky et al., 2015) or polysaccharides in case of pollen (Pummer et al., 2012). Furthermore several studies showed that INM are still ice active when the original carrier is detached or non viable (e.g., in the case of bacteria) (Kleber et al., 2007; Pummer et al., 2012, 2015; Hartmann et al., 2013; Augustin et al., 2013; Fröhlich-Nowoisky et al., 2015). So it is very likely that these INM are accumulated in the ground, where they come in contact with mineral dust particles. Already Schnell and Vali (1976) suggested that mineral dust particles may act as inert carriers for biological particles. Pratt et al. (2009) investigated 46 atmospheric cloud ice crystal residues with ATOFMS (Aerosol Time Of Flight Mass Spectrometer) and found that 60 % of the dust particles were likely a mixture of biological material and mineral dust. Also Michaud et al. (2014), investigating the residual particles in hail stones, found biological material to be attached to the surface of mineral dust particles. Therefore, there is some indication that the ascription of mineral dust to the atmospheric INP is, at least to a certain extent, due to unnoticed attached ice nucleating biological material (Conen et al., 2011). The question arises how the freezing ability of a mineral dust particle changes when there is some biological material attached to its surface. There are already some laboratory studies which confirm the enhanced freezing ability of soil dust due to the presence of biological

ACPD
15, 29639–29671, 2015

material (Conen et al., 2011; O'Sullivan et al., 2014; Tobo et al., 2014). But soil dust is a very inhomogeneous substance and it is very difficult to characterize which of its constituents is responsible for the freezing initiation, particularly as INM were found to be on the size of a few 10 nm only. Also, to quantify the freezing ability of an internal mixture of mineral dust and biological material it is advantageous to know the freezing ability of the individual materials. For this reason in the present study we mixed a well characterized mineral dust (illite-NX, Hiranuma et al., 2015) with well characterized biological material (birch pollen washing water, Pummer et al., 2012; Augustin et al., 2013) and investigated the immersion freezing ability of the resulting mixed particles, utilizing the Leipzig Aerosol Cloud Interaction Simulator (LACIS). In the following chapter the preparation of the mixture is described as well as the particle generation. We applied several methods for characterizing the mixing state of the generated aerosol, which are also described in the next chapter, together with the measurement set-up used for the ice nucleation measurements. Afterwards the results are presented and discussed.

2 Methods

2.1 Materials

To produce particles consisting of both dust and biological material, first a suspension containing both materials was prepared. For the experiments presented here illite-NX was chosen as the dust component, as this product has been used as a proxy for the natural dust composition found in the atmosphere (Hiranuma et al., 2015). Furthermore, the freezing ability of pure illite-NX particles was already investigated with LACIS in a previous study (Augustin-Bauditz et al., 2014). For the illite-NX suspensions 5 g of illite-NX powder were suspended in 100 mL of MilliQ water. After shaking the sample it was stored in the refrigerator for about 24 h. During that time large and heavy particles sedimented to the ground. An Eppendorf pipette was used to sample 25 mL from the top part of the suspension. This resulted in a suspension with an illite-NX concen-

ACPD
15, 29639–29671, 2015

tration of about 0.01 g mL^{-1}. The freezing ability of illite-NX particles generated from this suspension was measured with LACIS and compared to the freezing ability of dry generated illite-NX particles as presented in Augustin-Bauditz et al. (2014) (not shown here). No significant difference was observed.

As biological component, washing water from Swedish birch pollen (in the following BPWW) was used. The INM responsible for the freezing ability of BPWW are most likely polysaccharides (Pummer et al., 2012). The immersion freezing behavior of these INM was already investigated with LACIS and parameterizations are given in Augustin et al. (2013). The production of the BPWW suspension was done similar to that described in Augustin et al. (2013) but with a lower concentration of 1 g of pollen grains in 80 mL of MilliQ water. The birch pollen were mixed with the water and the pollen grains were then removed by filtration of the resulting suspension. After filtration the concentration of the Swedish birch pollen material in the suspension was about 0.004 g mL^{-1}.

The illite-NX suspension was mixed with the BPWW using the same amount of both, which resulted in a dust-bio-mixture to which we refer to in the following as illite–BPWW suspension. Concerning this illite–BPWW suspension, one should be aware of the following facts: A high percentage of the BPWW consists of soluble material which is released when the pollen grains are suspended in water. Thus the BPWW can be viewed as a suspension of INM (and other larger molecules) in a solution, rather than just a suspension in water. In contrast to that, the dust contains only a small amount of soluble material so the suspension consists mainly of solid particles and dilute water. These facts are important for the resulting mixing state of the internally mixed illite–BPWW particles and will be referred to again in the next section.

2.2 Particle generation and characterization

In Fig. 1 the generation pathway, starting from a suspension and ending with dry particles, is shown schematically. First an atomizer (following the design of TSI 3075) was used to generate droplets from the suspension. As mentioned above, the BPWW con-

ACPD
15, 29639–29671, 2015

tains a soluble fraction which was distributed in the whole suspension, so it is reasonable to assume that every droplet generated from the illite–BPWW suspension contained at least some soluble biological material, although not necessarily any INM. Most but maybe not all of these droplets also contained a mineral dust particle. After the atomization the droplets were dried by passing them through a silica gel diffusion dryer. Considering the above mentioned composition of the generated droplets, the resulting dry particles were most likely an internal mixture of illite-NX and BPWW material. There might have been also some particles consisting only of BPWW material but we expect no pure illite-NX particles in the generated aerosol. The dry particles were passed through a diffusion charger (85Kr) to achieve a bipolar charge distribution and afterwards size-selected using a differential mobility analyzer (DMA; Knutson and Whitby (1975); type "Vienna medium"). In the measurements presented here a mobility diameter of 500 nm was selected. Due to the use of a cyclone upstream of the DMA, the fraction of doubly charged particles contained in the aerosol is negligible: This was verified through measurements of the optical particle size distribution done downstream of the DMA using an UHSAS (Ultra-High Sensitivity Aerosol Spectrometer, Droplet Measurement Technologies). After size selection the aerosol stream was split and one part was always fed into a Condensation Particle Counter (CPC, TSI 3010) to measure the total particle number concentration. The remaining aerosol was then available for particle characterization (e.g., sampling on filters) and for the Leipzig Aerosol Cloud Interaction Simulator (LACIS).

To analyze the mixing state of the produced aerosol, several aerosol characterization methods were applied which will be briefly introduced in the following:

Volatility-Hygroscopicity Tandem Differential Mobility Analyser (VH-TDMA)

The volatility and hygroscopicity of the BPWW and illite-NX materials were used to infer the particle mixing state. In contrast to mineral dust, biological material is much more volatile and hygroscopic. Therefore, treatment with heat or humidity will change the size of particles consisting of biological material but likely will have a smaller ef-

ACPD
15, 29639–29671, 2015

fect on the mineral dust components. Measurements were performed with a custom-built VH-TDMA, which was composed of two DMAs and a CPC (TSI 3010) separated by a volatility (V-mode) and a humidity (H-mode) conditioning device. A mobility diameter of 500 nm, similar to that used for LACIS measurements, was selected with the first DMA. Monodisperse particles were then conditioned either in the thermodenuder section at 300 °C under dry conditions (10 % RH) or in the humidity section at 90 % RH at room temperature (20 °C). The residence times in the conditioning devices were approximately 2 s and 4 s for the V-mode and H-mode, respectively. The resulting particle size distributions obtained after conditioning were measured by the second DMA coupled to the CPC. The second DMA and the humidity section were confined in a temperature-controlled box at 20 °C. For the H-mode the sheath air of the second DMA was humidified to 90 % RH, too. The volatile "growth" factor VGF obtained from the V-mode is defined as: $\mathrm{VGF} = D_{\mathrm{p(300\,°C,10\,\%\,RH)}}/D_{\mathrm{p(20\,°C,10\,\%\,RH)}}$ where $D_{\mathrm{p(300\,°C,10\,\%\,RH)}}$ is the measured diameter after heating at 300 °C and $D_{\mathrm{p(20\,°C,10\,\%\,RH)}}$ the selected dry mobility diameter at ambient temperature. The hygroscopic growth factor HGF using the H-mode is defined in a similar way: $\mathrm{HGF} = D_{\mathrm{p(20\,°C,90\,\%\,RH)}}/D_{\mathrm{p(20\,°C,10\,\%\,RH)}}$ where $D_{\mathrm{p(20\,°C,90\,\%\,RH)}}$ is the measured diameter at 90 % RH. In this work, the distribution of growth factors refers to the growth factor probability density function (GF-PDF) and was fitted as a superposition of distinct Gaussian modes using the TDMAinv algorithm developed by Gysel et al. (2009). From comparing VGF and HGF distributions obtained for the pure and mixed particles, the fraction of internally mixed particles in the aerosol generated from the illite–BPWW suspensions can be derived.

Scanning Electron Microscope (SEM)

In cooperation with the Leibnitz institute of surface modification in Leipzig (IOM) filter samples of particles generated from the illite–BPWW suspension as well as from the pure illite-NX and BPWW suspensions were imaged with a SEM. With this technique we intended to examine visual differences between particles generated from the two

ACPD
15, 29639–29671, 2015

pure and from the illit–BPWW suspensions to see whether there are pure particles in the illite–BPWW aerosol.

Energy Dispersive X-ray analysis (EDX)

The Technical University of Darmstadt analyzed the generated particles using EDX. Particles were sampled on Bore-substrates and then sent to Darmstadt for the analysis. Analysis was performed in a FEI (Eindhoven, the Netherlands) Quanta 200 FEG Environmental Scanning Electron Microscope (ESEM) equipped with an energy-dispersive X-ray microanalysis system (EDX, Phoenix EDAX, Tilburg, the Netherlands). With this technique the elemental composition of individual particles is determined. The classification of the analyzed particles in pure illite particles, pure BPWW particles or internal mixture of both components was performed on base of the determined C/Si ratio. For particles with a C/Si ratio (based on netto count rate) larger than 10 or smaller than 0.1 external mixtures were assumed, all other particles are classified as internal illite / BPWW mixtures. Again, particles generated from the two pure suspensions were analyzed as well as particles generated from the illit–BPWW suspension.

Single Particle Laser Ablation Time-of-flight mass spectrometer (SPLAT)

Finally we also investigated the mixing state of the illite–BPWW aerosol via single particle mass spectrometry. Here, the instrument SPLAT (Kamphus et al., 2008) of the Max Planck Institute for Chemistry, Mainz, was used. For these experiments, particles were generated with the set-up described above and then examined in the SPLAT immediately after generation. This was done at first separately for an illite suspension and for BPWW, and then for the mixed particles generated from the illite–BPWW suspension. In the SPLAT, single particles are hit by a laser pulse which vaporizes and ionizes the compounds of the particle. A bipolar time-of-flight mass spectrometer is used to detect the ions. The composition and mixing state of the individual particles can then be inferred from their mass spectra. To decide whether a particle is an internal mixture

ACPD
15, 29639–29671, 2015

or a pure particle, the peak intensity ratio of selected marker peaks (Na/(Na + SiO)) was used (histograms of this ratio for the pure as well as for the mixed particles are shown in the Supplement). The experiments with the pure particles showed that values of this ratio between 0 and 0.1 occurred only for pure illite, while ratios larger than 0.65 were only observed for pure BPWW particles. Thus, particles with ratios between these threshold values are likely mixtures of both components. The uncertainties of this method can be estimated as follows: 25 % uncertainty originates from the amount of useful mass spectra per measurement (about 25 % of the mass spectra recorded in each experiment had to be discarded out due to insufficient ion count rate or wrong mass calibration). Additionally, 37 % of the pure illite values as well as 44 % of the pure BPWW values have intensity ratios in the intermediate range from 0.1 to 0.65. These uncertainties result in a possible underestimation of externally mixed particles of up to about a factor of 1.6 for illite and 1.8 for BPWW.

2.3 Freezing experiments

For the freezing experiments the laminar flow tube LACIS was utilized. In the inlet section of LACIS, the aerosol flow is combined isokinetically with a humidified sheath air flow such that the aerosol forms a beam of approximately 2 mm in diameter along the center line of the flow tube. Supersaturated conditions are achieved by cooling the tube walls, and result in activation of the particles to droplets, with each droplet containing one size segregated particle. Further downstream of the flow tube, these droplets then may freeze due to further cooling. For detailed information on the operation mode of LACIS see Stratmann et al. (2004) and Hartmann et al. (2011).

At the outlet of LACIS, TOPS-Ice (thermally-stabilized optical particle spectrometer, Clauss et al., 2013) is used to discriminate between frozen and unfrozen droplets, and to quantify the fraction of frozen droplet (f_{ice}, number of frozen droplets divided by the total number of frozen and unfrozen droplets). In the investigations presented here, f_{ice} was determined in the temperature range between ~ -17 and $-40\,^{\circ}C$.

ACPD
15, 29639–29671, 2015

3 Measurement results

In the following we will first describe the results of the methods that were used for obtaining information on the mixing state of the aerosol (3.1). Afterwards, we will describe the results of the immersion freezing experiments (3.2).

3.1 Mixing state of the produced aerosol

Several methods were applied to characterize the mixing state of the generated illite–BPWW aerosol. These were already introduced in Sect. 2.2 and their results will be discussed in the following.

The HGF and VGF distributions of the different particle types which were obtained from the VH-TDMA measurements are shown in Fig. 2. The values for the mean and spread of the different curves are given in Table 1. For the pure illite-NX particles (orange line) no change in size was observed for both treatments, which results in mean growth factors of approximatly 1. This confirms that the illite-NX contained no or only very little amounts of volatile or soluble material. In contrast to that, particles generated from the BPWW suspension (green line) showed a significant change in size for both treatments which lead to HGF and VGF of 1.38 and 0.57, respectively. The results for the particles generated from the illite–BPWW suspension (purple line) showed HGF and VGF values which are between those for the pure substances. It is also obvious that only one mode is present and that this mode shows no (for the VGF) or only little (for the HGF) overlap with the pure BPWW material. This suggests, that nearly all particles from the illite–BPWW suspension consisted of both, illite-NX and BPWW material or, in other words: all particles were internally mixed. Furthermore, the HGF values can be used to determine the hygroscopicity parameters κ of the different particle types (Petters and Kreidenweis, 2007). These κ values are 0, 0.176 and 0.017 for pure illite-NX, pure BPWW and internally mixed particles, respectively. For the κ of the internally mixed particles the simple mixing rule $\kappa_{mix} = \sum_i \epsilon_i \kappa_i$ can be applied (Petters and Kreidenweis, 2007). Here, ϵ_i depicts the amount of material i which has a κ value

ACPD
15, 29639–29671, 2015

of κ_i. With this it is possible to calculate the volume fraction of BPWW material on the internally mixed particles, which was found to be 9.7 %. Assuming spherical illite-NX particles surrounded by a smooth layer of BPWW material, the BPWW layer thickness would be 8 nm.

Examples of SEM images of the investigated particles are shown in Fig. 3. Particles generated from a BPWW suspension looked like viscous droplets (panel a). In contrast to that the illite-NX particles show a clear, nearly spherical shape (panel b). On a closer look, one recognizes that the illit-NX particles consists of small agglomerated plates. This structure was already described earlier by Broadley et al. (2012). The image of the particles generated from the illite–BPWW suspension is shown in the lower part of Fig. 3. In this example as well as in all other images that were taken, which are not all shown here, nearly none of the viscous droplets, which would indicate the presence of pure BPWW particles, could be observed in the illite–BPWW images. From the visual appearance, all particles resembled pure illite-NX particles. On the other hand, as described above, the generation method makes it very unlikely that pure illite-NX particles can be generated, as some material from the BPWW is always contained in the droplets generated from the atomizer. So we suggest, based on these images, that nearly all particles generated from illite–BPWW suspensions are internal mixtures, even if the BPWW material on the particles can not be identified visually. The VH-TDMA measurements already showed similar results and they indicated that the volume fraction of BPWW material is rather small compared to the volume fraction of illite-NX. As already assumed above, it might be that the illite-NX particles are covered with a thin 8 nm BPWW film, which is not optically visible in the microscope. It is also possible that due to the very low pressure (near vacuum) which is needed for the microscope imaging some of the more volatile BPWW compounds are evaporated.

The Darmstadt EDX analysis showed similar results as the SEM images from the IOM. Following the Si/C ratio 100 % of the analyzed particles generated from the illite–BPWW suspension were pure illite particles. An unambiguous identification of any BPWW material on the particles generated from this suspension was not possible

ACPD
15, 29639–29671, 2015

by EDX. Again, it can be argued that thin films of organic material were evaporated due to the vacuum in the microscope or that these films are too thin to be detectable by EDX.

The results of the SEM/EDX measurements for the mixing state of the particles generated from the illite–BPWW suspension can be summarized in the following way: no externaly mixed nonvolatile carbonaceous particles were found. The particles were rather determined to be pure illite particles, showing neither morphologically (by visualization) nor chemically (by EDX) any fingerprints for carbonaceous material. However, as the presence of the BPWW component was shown before by the VH-TDMA technique, these findings hint towards the biological material being present only as very thin carbonaceous films on the illite particles or by evaporation in the high vacuum SEM environment. In principle it is not possible to make a clear statement about the mixing state of the illite–BPWW particles from the SEM/EDX analysis. Nevertheless, as no pure BPWW particles were observed and as we do not expect pure illite-NX particles in the illite–BPWW aerosol, the assumption could be made that nearly all particles are internally mixed and that the BPWW material on the particles is rather small, which was already suggested by the VH-TDMA measurements.

For the illite–BPWW suspension 549 mass spectra were measured with the SPLAT, 150 of which had to be discarded due to insufficient ion count rate or wrong mass calibration. The remaining 399 mass spectra were used for the further analysis (the Na/(Na + SiO) histograms and data can be found in the Supplement). Of these spectra, around 328 (82 %) showed a ratio Na/(Na + SiO) between 0.1 and 0.65, indicating internal mixtures of illite-NX and BPWW material. Only 59 particles (14 %) appeared to be pure illite, and 16 (4 %) appeared to be pure BPWW in the SPLAT. However, the possible underestimation of the pure particles as mentioned above allows also values of 24 % pure illite and 7 % pure BPWW (which still means that 69 % of the particles are internally mixed). On the other hand, as discussed above, it is rather unlikely to find pure illite-NX particles in the aerosol generated from the illite–BPWW suspension. But as the VH-TDMA measurements as well as the SEM images and the EDX analysis

ACPD
15, 29639–29671, 2015

suggest that the amount of BPWW material on the particles might be rather small, it can not be ruled out that the SPLAT can not detect such small amounts of biological material and thus the amount of internally mixed particles is underestimated.

In Table 2 the results of all characterizations methods are summarized. It is obvious that the analysis of the mixing state of the generated illite–BPWW aerosol is not trivial and that it is bound to the limitations of the applied instruments. Nevertheless, all methods showed that a significant fraction, if not all, of the generated particles consisted of both, biological material and dust or, in other words, are internally mixed particles.

3.2 Immersion freezing experiments

In Fig. 4 the results of the immersion freezing experiments of the particles generated from the illite–BPWW suspension are shown (purple symbols). A first increase of the ice fraction with decreasing temperature can be observed at a temperature of about −17 °C. After this first steep increase the ice fraction curve becomes shallower and finally reaches a saturation level where no more droplets freeze with decreasing temperature. At about −36 °C, ice fraction starts to slightly rise again until the homogeneous freezing sets in (at about −38 °C). For a better understanding of the freezing behavior of the particles generated from the illite–BPWW suspension it is necessary to first understand the freezing behavior of the pure materials. Therefore, results of measurements from the pure 500 nm illite-NX and BPWW particles are shown in Fig. 4, too, as orange and green symbols, respectively. The straight lines in Fig. 4 represent modeled ice fractions for the different particle types. In the next section, it will be described, how these curves were obtained for the pure particles and how they can be combined to describe the ice nucleation behavior of the internally mixed particles.

ACPD
15, 29639–29671, 2015

4 Theoretical description and discussion

In the following, we will describe the modeling of the ice nucleation measurements and will show what can be learned from that. For this, the SBM in the version introduced in Niedermeier et al. (2015) will be used. First we will explain the basics of this model, then we will introduce the parameterizations for the pure substances, and finally the ice nucleation of the mixed illite–BPWW particles will be modeled.

4.1 Basics of the Soccerball model

In general it is assumed that freezing is induced by single ice nucleating entities. These entities can be e.g. special sites on the surface of a particle (as it is assumed for mineral dust particles) or, in the case of biological material, single INM. In any case, the ice nucleating entity has a defined two dimensional surface area s_{site}. A specific contact angle θ is assigned to each of the ice nucleating entities which determines the ice nucleation ability of this particular entity in terms of a nucleation rate coefficient j_{het} based on classical nucleation theory (Zobrist et al., 2007). The contact angle θ of each surface site is determined by a Gaussian probability density function with a mean value μ_θ and a standard deviation σ_θ.

$$p(\theta) = \frac{1}{\sqrt{2\pi}\sigma_\theta} \exp\left(-\frac{(\theta-\mu_\theta)^2}{2\sigma_\theta^2}\right) \quad (1)$$

The probability P_{unfr} of a single entity to not initiate ice nucleation at a a certain temperature T and a certain time t is defined as:

$$P_{\mathrm{unfr}}(T,\mu_\theta,\sigma_\theta,t) = \int_0^x p_\theta \exp(-j_{\mathrm{het}}(T,\theta)s_{\mathrm{site}}t)\mathrm{d}\theta$$

ACPD
15, 29639–29671, 2015

$$+ \int_{-\infty}^{0} p_\theta \exp(-j_{\text{het}}(T, \theta = 0) s_{\text{site}} t) \mathrm{d}\theta$$

$$+ \int_{x}^{\infty} p_\theta \exp(-j_{\text{het}}(T, \theta = \pi) s_{\text{site}} t) \mathrm{d}\theta \quad (2)$$

As a next step, we consider a population of droplets, with each droplet containing a single particle and all particles having the same size. It is assumed that the ice nucleating entities are Poisson distributed over the particle population. Thus the average number of ice nucleating entities per particle is defined by the expected value of the Poisson distribution λ (Hartmann et al., 2013). Depending on λ, each particle contains none, one or even multiple ice nucleating entities and all entities have the same freezing probability. With this, the probability $P_{\text{unfr},\lambda}$ for droplets to remain unfrozen is given by:

$$P_{\text{unfr},\lambda}(T, \mu_\theta, \sigma_\theta, \lambda, t) = \exp\left(-\lambda\left(1 - P_{\text{unfr}}(T, \mu_\theta, \sigma_\theta, t)\right)\right) \quad (3)$$

The ice fraction, which is identical to the freezing probability $P_{\text{fr},\lambda}$ follows with:

$$f_{\text{ice}}(T, \mu_\theta, \sigma_\theta, \lambda, t) = 1 - P_{\text{unfr},\lambda} \quad (4)$$

Equation (4) represents the combination of the original SBM from Niedermeier et al. (2014) and the CHESS model from Hartmann et al. (2013) and was derived in detail in Niedermeier et al. (2015). λ is a material and size depending parameter and its determination is dependent on the freezing behavior of the investigated material.

4.2 Immersion freezing properties of BPWW particles

For the freezing behavior of BPWW (green line in Fig. 4) it was observed that the ice fraction reaches a saturation range below one (Augustin et al., 2013), which means that

ACPD
15, 29639–29671, 2015

at a certain temperature no further increase in ice fraction with decreasing temperature is observed. It is known that single INM are responsible for the freezing behavior of the BPWW material. The occurrence of a saturation range below one implies that not all of the particles generated from a BPWW suspension contain an INM (a similar behavior was observed for Snomax in Hartmann et al., 2013). In those cases, λ can be directly calculated from the ice fraction f^*_{ice} observed in the saturation range, with: $\lambda = -\ln(1 - f^*_{\mathrm{ice}})$.

In Augustin et al. (2013) it was possible to describe the λ value of the BPWW by both, a linear particle volume dependence and a linear particle surface area dependence, where a surface area dependence yielded a slightly better regression coefficient (surface area: $r = 0.9918$, and volume: $r = 0.9275$). This was somehow surprising as it was expected that the BPWW particles are fully soluble and thus should show a clear linear volume dependence (as for example in the case of Snomax; Hartmann et al., 2013). In Augustin et al. (2013) it was speculated that the BPWW contains some slowly dissolving material and that the generated particles may need more time than the few seconds they have in LACIS to dissolve completely, which would explain the surface dependence of λ.

It should be mentioned here that the Swedish birch pollen washing water which was used in this study contains two different INM (called INM-α and INM-β), which are internally mixed (Augustin et al., 2013). So for the BPWW used in this study Eq. (3) changes to:

$$P^{\mathrm{BPWW}}_{\mathrm{unfr},\lambda}(T, \mu_\theta, \sigma_\theta, \lambda, t) = \exp\Big(-\lambda_\alpha\big(1 - P_{\mathrm{unfr},\alpha}\big) - \lambda_\beta\big(1 - P_{\mathrm{unfr},\beta}\big)\Big) \quad (5)$$

The two different INM are the reason for the change in the slope of the BPWW ice fraction curve at around −20 °C. The values for μ_θ and σ_θ for both INM contained in the BPWW were taken from Augustin et al. (2013) and are given in Table 3. The size of a single INM was estimated to be 10 nm (Pummer et al., 2012). Assuming spherical INM this leads to a s_{site} of 3.14×10^{-16} m^2. As explained above the λ values of INM-α and INM-β can be described by both a linear volume dependence and a linear surface

ACPD
15, 29639–29671, 2015

area dependence. The relations between λ and particle volume for INM-α and INM-β can be described as follows:

$$-\lambda_\alpha = 6.76 \times 10^{18}\,\mathrm{m}^{-3} \times D_\mathrm{p}^3 \text{ and } \lambda_\beta = 1.31 \times 10^{18}\,\mathrm{m}^{-3} \times D_\mathrm{p}^3.$$

When assuming a surface area dependence the relations are:

$$-\lambda_\alpha = 3.30 \times 10^{12}\,\mathrm{m}^{-2} \times D_\mathrm{p}^2 \text{ and } \lambda_\beta = 6.65 \times 10^{11}\,\mathrm{m}^{-2} \times D_\mathrm{p}^2.$$

These values differ a little from the respective values given in Augustin et al. (2013). The reason for that is that for the measurements done for the here presented study (meaning both, those of pure BPWW and those for mixed illite–BPWW particles) a new birch pollen batch was used. It is not surprising that due to natural variability the number of INM per particle differs from batch to batch. But the ice nucleation properties (μ_θ and σ_θ) are similar, as the same INM are present.

4.3 Immersion freezing properties of illite-NX particles

In contrast to the BPWW particles we did not observe a saturation range for the frozen fraction for the illite-NX particles (Augustin-Bauditz et al., 2014). But, due to the lower ice nucleating ability, it could be plausible that homogeneous ice nucleation, which is dominant for $T < -38\,^{\circ}\mathrm{C}$, perhaps masks a potential leveling off of the frozen fraction curves. Therefore, we also used the presented procedure for representing the ice nucleating ability of the pure illite-NX particles (orange line in Fig. 4). To do so, the following assumptions were made. First, the λ value of illite-NX is assumed to be smaller than the determined λ value for feldspar given in Niedermeier et al. (2015). This is a reasonable assumption as K-feldspar was observed to be the most ice active mineral dust found so far (Atkinson et al., 2013; Augustin-Bauditz et al., 2014). Second, we assume that λ is directly correlated to the particle surface area, as for mineral dust it is assumed that the ice nucleating entities are special sites on the surface of the particle. This correlation between λ and particle surface area was already observed

ACPD
15, 29639–29671, 2015

for feldspar particles (Niedermeier et al., 2015). Due to these assumptions we could distinctly narrow the range of the possible λ parameter. For a s_{site} of 10^{-14} m^2 as used in Niedermeier et al. (2015), the best fit between measured and modeled data was obtained for $\lambda_{illite} = 3.25 \times 10^{12}\,m^{-2} \times D_p^2$. The resulting μ_θ and σ_θ are given in Table 3.

4.4 Immersion freezing properties of illite–BPWW particles

The comparison between the freezing behavior of the particles generated from the illite–BPWW suspension and the pure substances indicates that it is possible to explain the immersion freezing behavior of the mixture by the freezing abilities of the pure substances. Down to roughly −30 °C, the temperature range at which the first steep increase is observed, and also the subsequent course of the ice fraction, are identical to those of pure BPWW particles. The second increase in the frozen fraction below −30 °C, from roughly 0.2 to above 0.3, occurs in a temperature range for which the ice nucleation is observed for pure illite-NX particles. In other words the freezing behavior of the mixed particles appears as superposition of the single substances' freezing behaviors, and the most ice active ice nucleation entity within the particle will dominate the freezing process. For the 500 nm illite–BPWW particles considered here the INM of the BPWW material are the dominant ice nucleation entity in the temperature range between −17 and −30 °C. At this point, it is worth mentioning that although we assume that every particle contains some material from the BPWW, not every particle will contain an INM, as already pure 500 nm BPWW particles did not all contain an INM. Hence in some illite–BPWW particles, it will be the illite which induces droplet freezing.

In the following, we model the ice nucleation behavior of the illite–BPWW particles based on the already existing SBM parameters (μ_θ and σ_θ from Table 3) for the pure substances. Therefore, we first consider that all particles are internally mixed (see discussion in Sect. 3.1). As independent probabilities are multiplicative, the $P_{unfr,\,mix}$ is calculated as follows:

$$P_{unfr,mix}(T, \mu_\theta, \sigma_\theta, \lambda, t) = P_{unfr,\lambda}^{illite} \times P_{unfr,\lambda}^{BPWW} \quad (6)$$

ACPD
15, 29639–29671, 2015

With that the ice fraction can be determined as follows:

$$f_{\text{ice}}(T, \mu_\theta, \sigma_\theta, \lambda, t) = 1 - P_{\text{unfr, mix}} \quad (7)$$

Equation (7) now represents the freezing behavior of particles, which consist of both, illite-NX and BPWW material, assuming that the freezing behavior of the pure substances remains unchanged, even when they are mixed. As already mentioned, the μ_θ and σ_θ values of the pure substances are independent of the particle size. In contrast to that the parameters λ_α, λ_β and λ_{illite} change when the particle size changes.

From the VH-TDMA measurements we know that the soluble volume fraction of the BPWW material in the internally mixed particle is approximately 9.7 %. As mentioned above it might be that the BPWW material on the illite-NX material does not fully dissolve during the few seconds in LACIS, where the particle is immersed in a droplet. In the following we want to discuss three different behaviors, the internally mixed particles may show during the freezing experiments (Fig. 5). Case a depicts an extreme case, where the illite-NX particle is fully covered with BPWW material and the BPWW material does not dissolve at all. Only the BPWW material is exposed to the water and can trigger the freezing process. In this case the internally mixed particles would behave exactly like pure 500 nm BPWW particle (green line in Fig. 4). Obviously this case overestimates the measured ice fractions of the illite–BPWW particles. Case b shows another extreme case. Here the whole BPWW material is dissolved in the droplet. Assuming the volume fraction of BPWW material on the illite–BPWW particles to be 9.7 %, we can calculate the λ values of the BPWW material (assuming λ to be volume depended) as well as λ_{illite} for the remaining spherical illite-NX particle. The resulting ice fraction curve is shown in Fig. 4 as a grey line. It is obvious that in this case the ice fraction of the illite–BPWW particles is underestimated. We can conclude from this that the real case is an intermediate case of a and b (panel c in Fig. 5). The BPWW material dissolves partly, as it was already suggested in Augustin et al. (2013). For this case the size parameters can not be calculated directly as we have no information of how much of the BPWW material will dissolve and how much will still cover the illite-

ACPD
15, 29639–29671, 2015

NX core. So we fit Eq. (7) to the measured data with λ_α, λ_β and λ_{illite} beeing the fit parameters, where the relation between λ_α and λ_β remains the same as derived from the measurements of the pure BPWW. This leads to the following results:

$-\lambda_\alpha = 0.2062, \lambda_\beta = 0.0412, \lambda_{\text{illite}} = 0.3293$

This is depicted as purple line in Fig. 4, and fits the course of the measured data well over the whole temperature range. It should be noted at this point that in the model the ice nucleation properties (μ_θ and σ_θ) of both materials have not been changed and still are the same as for the pure materials. So with the modeled ice fraction curves we can confirm that it is possible to explain the course of the immersion freezing behavior of the mixture by the freezing abilities of the pure substances.

5 Conclusions

Several studies showed that mineral dust particles can act as carriers for biological material. Up to now it was not shown clearly how a single particle which consists of both, mineral dust and biological material, behaves in terms of ice nucleation.

In this study we showed that it is possible to quantitatively describe the freezing behavior of particles generated from a illite–BPWW suspension, based on parameters (mean values μ_θ and standard deviations σ_θ) of the pure substances. In other words, the freezing behavior of the mixed particles appears as superposition of the single substances' freezing behaviors and for a droplet containing such a mixed particle, the most active freezing entity in the droplet will control the freezing process at a certain temperature. For the internally mixed particles presented here, this means that if there is an INM located on the surface of an illite-NX particle, this INM will initiate the freezing of the droplet already at much higher temperatures than the pure illite-NX particle.

However, already for the here examined particles generated in the laboratory under well defined conditions, it was difficult to determine the mixing state of the particles, and it was seen that particularly the biological fraction of a mixed bio-dust particle

ACPD
15, 29639–29671, 2015

might be overlooked. Atmospheric measurements are usually even more challenging, and therefore ice nucleation attributed to mineral dust in the past occasionally might have been due to an undetected biological component.

Based on our results the following advices can be given for the modeling of atmospheric ice nucleation. On the one hand it is not necessary to define new parameterizations for dust-bio-mixtures as these particles, depending on actual composition, induce freezing similar to the pure substances. On the other hand, this implies that for proper modeling, the knowledge concerning the number of mineral and biological IN and their mixing state is highly desirable. To find the respective atmospherically relevant values is still a big challenge as the particle characterization methods are limited in their ability to detect rarely occurring materials.

The Supplement related to this article is available online at doi:10.5194/acpd-15-29639-2015-supplement.

Acknowledgements. This work is partly funded by the German Research Foundation (DFG projects WE 4722/1-1, WE 4722/1-2, EB 383/3-1, EB 383/3-2, SCHN 1138/2-1 and SCHN 1138/2-2) within the DFG Research Unit FOR 1525 INUIT. We thank Dennis Niedermeier for discussions. We also thank the IOM and Andrea Prager for the SEM images. J. Schneider and S. Schmidt thank Oliver Appel for support during the SPLAT measurements.

References

Atkinson, J. D., Murray, B. J., Woodhouse, M. T., Whale, T. F., Baustian, K. J., Carslaw, K. S., Dobbie, S., O'Sullivan, D., and Malkin, T. L.: The importance of feldspar for ice nucleation by mineral dust in mixed-phase clouds, Nature, 498, 355–358, doi:10.1038/nature12278, 2013. 29655

Augustin, S., Wex, H., Niedermeier, D., Pummer, B., Grothe, H., Hartmann, S., Tomsche, L., Clauss, T., Voigtländer, J., Ignatius, K., and Stratmann, F.: Immersion freezing of birch pollen

ACPD
15, 29639–29671, 2015

washing water, Atmos. Chem. Phys., 13, 10989–11003, doi:10.5194/acp-13-10989-2013, 2013. 29641, 29642, 29643, 29653, 29654, 29655, 29657, 29666

Augustin-Bauditz, S., Wex, H., Kanter, S., Ebert, M., Niedermeier, D., Stolz, F., Prager, A., and Stratmann, F.: The immersion mode ice nucleation behavior of mineral dusts: a comparison of different pure and surface modified dusts, Geophys. Res. Lett., 41, 7375–7382, doi:10.1002/2014gl061317, 2014. 29641, 29642, 29643, 29655, 29666

Broadley, S. L., Murray, B. J., Herbert, R. J., Atkinson, J. D., Dobbie, S., Malkin, T. L., Condliffe, E., and Neve, L.: Immersion mode heterogeneous ice nucleation by an illite rich powder representative of atmospheric mineral dust, Atmos. Chem. Phys., 12, 287–307, doi:10.5194/acp-12-287-2012, 2012. 29649

Bühl, J., Ansmann, A., Seifert, P., Baars, H., and Engelmann, R.: Toward a quantitative characterization of heterogeneous ice formation with lidar/radar: comparison of CALIPSO/CloudSat with ground-based observations, Geophys. Res. Lett., 40, 4404–4408, doi:10.1002/grl.50792, 2013. 29641

Clauss, T., Kiselev, A., Hartmann, S., Augustin, S., Pfeifer, S., Niedermeier, D., Wex, H., and Stratmann, F.: Application of linear polarized light for the discrimination of frozen and liquid droplets in ice nucleation experiments, Atmos. Meas. Tech., 6, 1041–1052, doi:10.5194/amt-6-1041-2013, 2013. 29647

Conen, F., Morris, C. E., Leifeld, J., Yakutin, M. V., and Alewell, C.: Biological residues define the ice nucleation properties of soil dust, Atmos. Chem. Phys., 11, 9643–9648, doi:10.5194/acp-11-9643-2011, 2011. 29641, 29642

DeMott, P. J., Cziczo, D. J., Prenni, A. J., Murphy, D. M., Kreidenweis, S. M., Thomson, D. S., Borys, R., and Rogers, D. C.: Measurements of the concentration and composition of nuclei for cirrus formation, P. Natl. Acad. Sci. USA, 100, 14655–14660, doi:10.1073/pnas.2532677100, 2003. 29640

Fröhlich-Nowoisky, J., Hill, T. C. J., Pummer, B. G., Yordanova, P., Franc, G. D., and Pöschl, U.: Ice nucleation activity in the widespread soil fungus *Mortierella alpina*, Biogeosciences, 12, 1057–1071, doi:10.5194/bg-12-1057-2015, 2015. 29641

Gysel, M., McFiggans, G. B., and Coe, H.: Inversion of tandem differential mobility analyser (TDMA) measurements, J. Aerosol Sci., 40, 134–151, doi:10.1016/j.jaerosci.2008.07.013, 2009. 29645

Hartmann, S., Niedermeier, D., Voigtländer, J., Clauss, T., Shaw, R. A., Wex, H., Kiselev, A., and Stratmann, F.: Homogeneous and heterogeneous ice nucleation at LACIS: operating

ACPD
15, 29639–29671, 2015

principle and theoretical studies, Atmos. Chem. Phys., 11, 1753–1767, doi:10.5194/acp-11-1753-2011, 2011. 29647
Hartmann, S., Augustin, S., Clauss, T., Wex, H., Šantl-Temkiv, T., Voigtländer, J., Niedermeier, D., and Stratmann, F.: Immersion freezing of ice nucleation active protein complexes, Atmos. Chem. Phys., 13, 5751–5766, doi:10.5194/acp-13-5751-2013, 2013. 29641, 29653, 29654
Hiranuma, N., Augustin-Bauditz, S., Bingemer, H., Budke, C., Curtius, J., Danielczok, A., Diehl, K., Dreischmeier, K., Ebert, M., Frank, F., Hoffmann, N., Kandler, K., Kiselev, A., Koop, T., Leisner, T., Möhler, O., Nillius, B., Peckhaus, A., Rose, D., Weinbruch, S., Wex, H., Boose, Y., DeMott, P. J., Hader, J. D., Hill, T. C. J., Kanji, Z. A., Kulkarni, G., Levin, E. J. T., McCluskey, C. S., Murakami, M., Murray, B. J., Niedermeier, D., Petters, M. D., O'Sullivan, D., Saito, A., Schill, G. P., Tajiri, T., Tolbert, M. A., Welti, A., Whale, T. F., Wright, T. P., and Yamashita, K.: A comprehensive laboratory study on the immersion freezing behavior of illite NX particles: a comparison of 17 ice nucleation measurement techniques, Atmos. Chem. Phys., 15, 2489–2518, doi:10.5194/acp-15-2489-2015, 2015. 29642
Kamphus, M., Ettner-Mahl, M., Brands, M., Curtius, J., Drewnick, F., and Borrmann, S.: Comparison of two aerodynamic lenses as an inlet for a single particle laser ablation mass spectrometer, Aerosol Sci. Tech., 42, 970–980, doi:10.1080/02786820802372158, 2008. 29646
Kanitz, T., Seifert, P., Ansmann, A., Engelmann, R., Althausen, D., Casiccia, C., and Rohwer, E. G.: Contrasting the impact of aerosols at northern and southern midlatitudes on heterogeneous ice formation, Geophys. Res. Lett., 38, L17802, doi:10.1029/2011gl048532, 2011. 29641
Kleber, M., Sollins, P., and Sutton, R.: A conceptual model of organo-mineral interactions in soils: self-assembly of organic molecular fragments into zonal structures on mineral surfaces, Biogeochemistry, 85, 9–24, doi:10.1007/s10533-007-9103-5, 2007. 29641
Knutson, E. O. and Whitby, K. T.: Aerosol classification by electric mobility: apparatus, theory, and applications, J. Aerosol Sci., 6, 443–451, doi:10.1016/0021-8502(75)90060-9, 1975. 29644
Kumai, M.: Snow crystals and the identification of the nuclei in the northern United-States of America, J. Meteorol., 18, 139–150, doi:10.1175/1520-0469(1961)018<0139:scatio>2.0.co;2, 1961. 29640
Maki, L. R., Galyan, E. L., Chang-Chien, M., and Caldwell, D. R.: Ice nucleation induced by pseudomonas-syringea, Applied Microbiology, 28, 456–459, 1974. 29641

ACPD
15, 29639–29671, 2015

Michaud, A. B., Dore, J. E., Leslie, D., Lyons, W. B., Sands, D. C., and Priscu, J. C.: Biological ice nucleation initiates hailstone formation, J. Geophys. Res.-Atmos., 119, 12186–12197, doi:10.1002/2014jd022004, 2014. 29641

Morris, C. E., Sands, D. C., Vinatzer, B. A., Glaux, C., Guilbaud, C., Buffiere, A., Yan, S., Dominguez, H., and Thompson, B. M.: The life history of the plant pathogen *Pseudomonas syringae* is linked to the water cycle, Isme J., 2, 321–334, doi:10.1038/ismej.2007.113, 2008. 29641

Murray, B. J., O'Sullivan, D., Atkinson, J. D., and Webb, M. E.: Ice nucleation by particles immersed in supercooled cloud droplets, Chem. Soc. Rev., 41, 6519–6554, doi:10.1039/c2cs35200a, 2012. 29641

Niedermeier, D., Ervens, B., Clauss, T., Voigtländer, J., Wex, H., Hartmann, S., and Stratmann, F.: A computationally efficient description of heterogeneous freezing: a simplified version of the Soccerball model, Geophys. Res. Lett., 41, 736–741, doi:10.1002/2013gl058684, 2014. 29653

Niedermeier, D., Augustin-Bauditz, S., Hartmann, S., Wex, H., Ignatius, K., and Stratmann, F.: Can we define an asymptotic value for the ice active surface site density for heterogeneous ice nucleation?, J. Geophys. Res.-Atmos., 120, 5036–5046, doi:10.1002/2014JD022814, 2015. 29652, 29653, 29655, 29656

O'Sullivan, D., Murray, B. J., Malkin, T. L., Whale, T. F., Umo, N. S., Atkinson, J. D., Price, H. C., Baustian, K. J., Browse, J., and Webb, M. E.: Ice nucleation by fertile soil dusts: relative importance of mineral and biogenic components, Atmos. Chem. Phys., 14, 1853–1867, doi:10.5194/acp-14-1853-2014, 2014. 29642

Petters, M. D. and Kreidenweis, S. M.: A single parameter representation of hygroscopic growth and cloud condensation nucleus activity, Atmos. Chem. Phys., 7, 1961–1971, doi:10.5194/acp-7-1961-2007, 2007. 29648

Pratt, K. A., DeMott, P. J., French, J. R., Wang, Z., Westphal, D. L., Heymsfield, A. J., Twohy, C. H., Prenni, A. J., and Prather, K. A.: In situ detection of biological particles in cloud ice-crystals, Nat. Geosci., 2, 397–400, doi:10.1038/ngeo521, 2009. 29640, 29641

Pummer, B. G., Bauer, H., Bernardi, J., Bleicher, S., and Grothe, H.: Suspendable macromolecules are responsible for ice nucleation activity of birch and conifer pollen, Atmos. Chem. Phys., 12, 2541–2550, doi:10.5194/acp-12-2541-2012, 2012. 29641, 29642, 29643, 29654

Pummer, B. G., Budke, C., Augustin-Bauditz, S., Niedermeier, D., Felgitsch, L., Kampf, C. J., Huber, R. G., Liedl, K. R., Loerting, T., Moschen, T., Schauperl, M., Tollinger, M., Morris, C. E.,

ACPD
15, 29639–29671, 2015

Wex, H., Grothe, H., Pöschl, U., Koop, T., and Fröhlich-Nowoisky, J.: Ice nucleation by water-soluble macromolecules, Atmos. Chem. Phys., 15, 4077–4091, doi:10.5194/acp-15-4077-2015, 2015. 29641

Schnell, R. C. and Vali, G.: Biogenic ice nuclei: Part I. Terrestrial and marine sources, J. Atmos. Sci., 33, 1554–1564, doi:10.1175/1520-0469(1976)033<1554:BINPIT>2.0.CO;2, 1976. 29641

Seifert, P., Ansmann, A., Mattis, I., Wandinger, U., Tesche, M., Engelmann, R., Mueller, D., Perez, C., and Haustein, K.: Saharan dust and heterogeneous ice formation: eleven years of cloud observations at a central European EARLINET site, J. Geophys. Res.-Atmos., 115, D20201, doi:10.1029/2009jd013222, 2010. 29641

Stratmann, F., Kiselev, A., Wurzler, S., Wendisch, M., Heintzenberg, J., Charlson, R. J., Diehl, K., Wex, H., and Schmidt, S.: Laboratory studies and numerical simulations of cloud droplet formation under realistic supersaturation conditions, J. Atmos. Ocean. Tech., 21, 876–887, doi:10.1175/1520-0426(2004)021<0876:lsanso>2.0.co;2, 2004. 29647

Tobo, Y., DeMott, P. J., Hill, T. C. J., Prenni, A. J., Swoboda-Colberg, N. G., Franc, G. D., and Kreidenweis, S. M.: Organic matter matters for ice nuclei of agricultural soil origin, Atmos. Chem. Phys., 14, 8521–8531, doi:10.5194/acp-14-8521-2014, 2014. 29642

Wolber, P. K., Deininger, C. A., Southworth, M. W., Vandekerckhove, J., Vanmontagu, M., and Warren, G. J.: Identification and purification of a bacterial ice-nucleation protein, P. Natl. Acad. Sci. USA, 83, 7256–7260, doi:10.1073/pnas.83.19.7256, 1986. 29641

Zobrist, B., Koop, T., Luo, B. P., Marcolli, C., and Peter, T.: Heterogeneous ice nucleation rate coefficient of water droplets coated by a nonadecanol monolayer, J. Phys. Chem.-US, 111, 2149–2155, doi:10.1021/jp066080w, 2007. 29652

ACPD
15, 29639–29671, 2015

Table 1. Mean value and spread of the HGF and VGF distribution for the different heated (V) and humidified (H) particle types. The selected size prior to the treatment was 500 nm.

	suspension	mean	spread
HGF	illite-NX	0.99	0.01
	BPWW	1.38	0.07
	illite–BPWW	1.05	0.05
VGF	illite-NX	0.99	0.01
	BPWW	0.56	0.02
	illite–BPWW	0.87	0.01

ACPD
15, 29639–29671, 2015

Table 2. Summary of the results of all characterization methods. The amounts of pure and internally mixed particles are given in %. For SEM and EDX no clear statement could be given, so the assumed values are given in parentheses. The values in squared brackets depict the possible SPLAT results if the underestimations of pure particles are implemented.

	SEM	EDX	SPLAT	HTDMA	VTDMA
pure illite	(0)	(0)	14 [24]	0	0
pure BPWW	(0)	(0)	4 [7]	< 1	0
internal mixture	(100)	(100)	82 [69]	> 99	100

ACPD
15, 29639–29671, 2015

Table 3. Soccerball model parameters used for the calculations shown in Fig. 4. The values for μ_θ and σ_θ are determined from former measurements with the pure substances (Augustin et al., 2013 for the BPWW parameters and Augustin-Bauditz et al., 2014 for the illite-NX parameters).

	μ_θ [rad]	σ_θ [rad]
pure illite	1.9031	0.2743
pure BPWW (INM-α)	1.016	0.0803
pure BPWW (INM-β)	0.834	0.0005

ACPD
15, 29639–29671, 2015

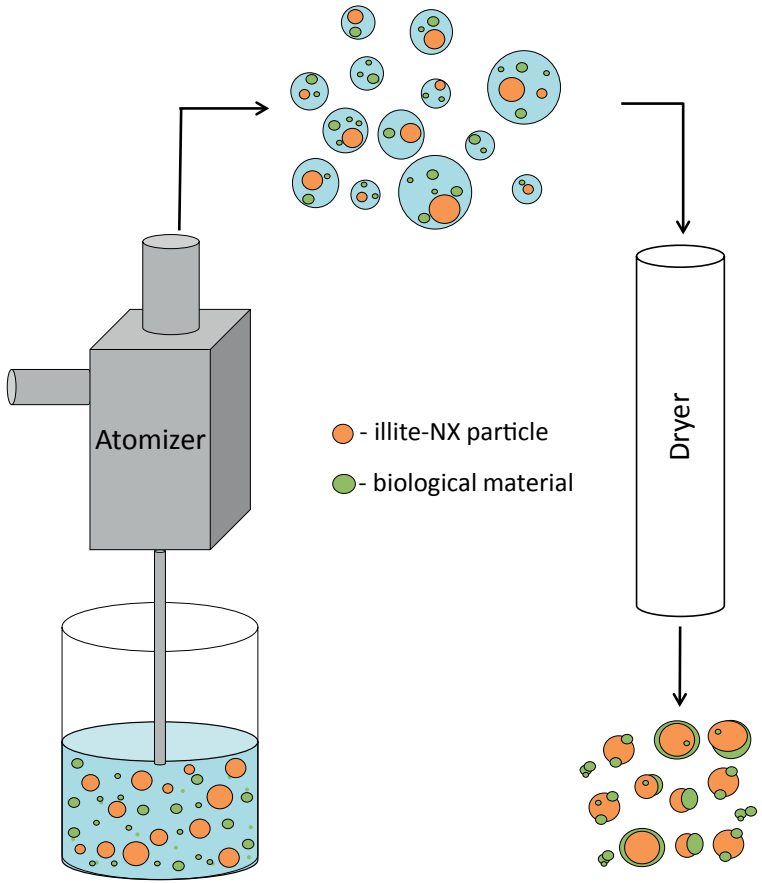

Figure 1. Schematic of the particle generation method used in this study.

ACPD
15, 29639–29671, 2015

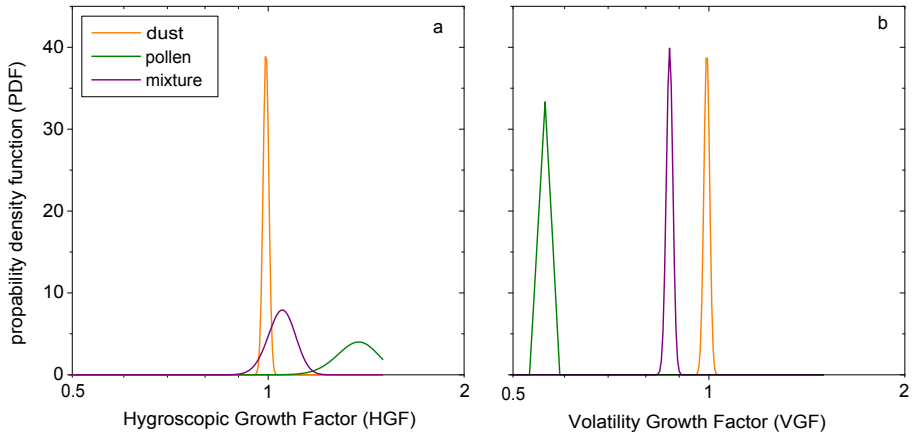

Figure 2. Left part: probability density function (PDF) of the hygroscopic growth factor (HGF) determined from the VH-TDMA measurements at 90 % relative humidity. Right part: PDF of the volatile "growth" factor (VGF) determined from the VH-TDMA measurements at 300 °C.

ACPD
15, 29639–29671, 2015

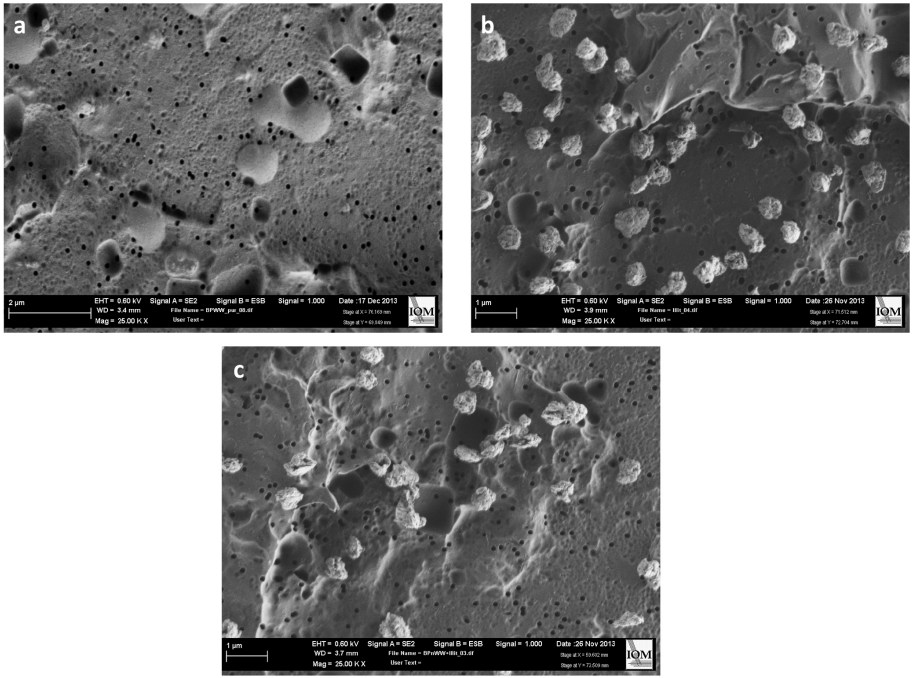

Figure 3. Examples of SEM images of the different suspensions. **(a)** BPWW, **(b)** illite-NX, **(c)** illite–BPWW.

ACPD
15, 29639–29671, 2015

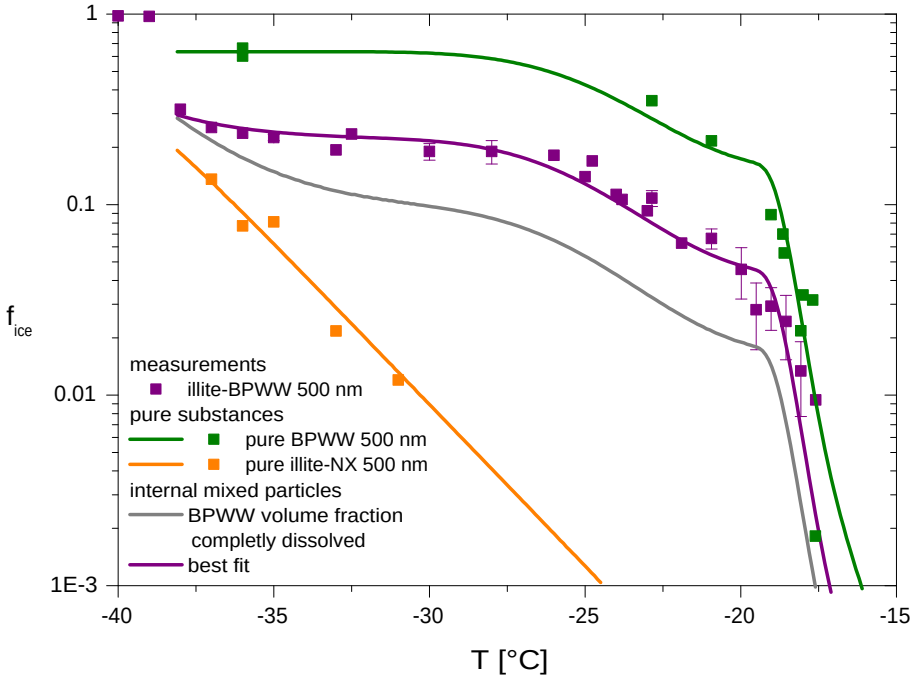

Figure 4. Results of the immersion freezing experiments of particles with an mobility diameter of 500 nm generated from the illite–BPWW-suspension as well as from the pure illite-NX and BPWW particles (purple, orange and green symbols, respectively). Error bars are the standard deviation of the experiments and were obtained for temperatures with at least three measurements. The green and the orange line represent the freezing ability of pure BPWW and illite-NX particles, respectively (500 nm mobility diameter) based on the SBM parameters determined from former investigations. The grey line represents an extreme case where all the available BPWW material (9.7 % volume fraction) has been dissolved in the droplet. The purple line represents the freezing behavior of internally mixed particles which was fitted to the measured data.

ACPD
15, 29639–29671, 2015

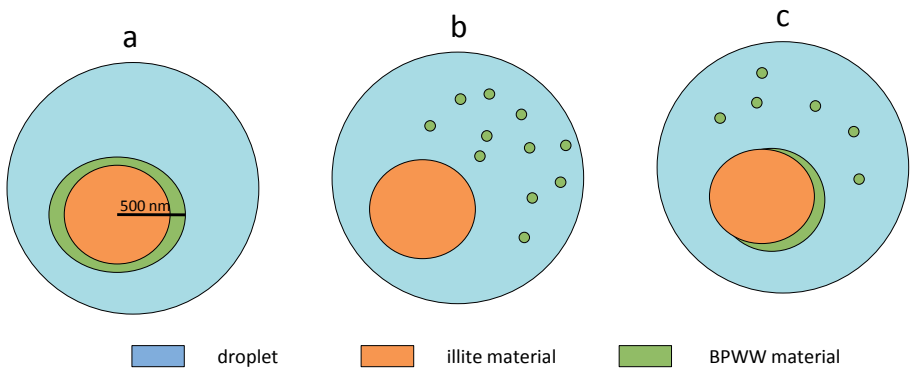

Figure 5. Theoretical forms of mixing of a spherical internally mixed illite–BPWW particle. **(a)** The illite-NX particle is completely covered with BPWW material which does not dissolve in the droplet. **(b)** The BPWW material is completely dissolved in the droplet. **(c)** The BPWW material is partly dissolved and partly still on the illite-NX particle.

ACPD
15, 29639–29671, 2015